ACS APPLIED MATERIALS & INTERFACES

Research Article

www.acsami.org

Modulated Two-Dimensional Charge-Carrier Density in $LaTiO_3$–Layer-Doped $LaAlO_3/SrTiO_3$ Heterostructure

Safdar Nazir, Camille Bernal, and Kesong Yang*

Department of NanoEngineering, University of California, San Diego, 9500 Gilman Drive, Mail Code 0448, La Jolla, California 92093-0448, United States

ABSTRACT: The highly mobile two-dimensional electron gas (2DEG) formed at the polar/nonpolar $LaAlO_3/SrTiO_3$ (LAO/STO) heterostructure (HS) is a matter of great interest because of its potential applications in nanoscale solid-state devices. To realize practical implementation of the 2DEG in device design, desired physical properties such as tuned charge carrier density and mobility are necessary. In this regard, polar perovskite-based transition metal oxides can act as doping layers at the interface and are expected to tune the electronic properties of 2DEG of STO-based HS systems dramatically. Herein, we investigated the doping effects of $LaTiO_3$(LTO) layers on the electronic properties of 2DEG at n-type $(LaO)^{+1}/(TiO_2)^0$ interface in the LAO/STO HS using spin-polarized density functional theory calculations. Our results indicate an enhancement of orbital occupation near the Fermi energy, which increases with respect to the number of LTO unit cells, resulting in a higher charge carrier density of 2DEG than that of undoped system. The enhanced charge carrier density is attributed to an extra electron introduced by the Ti $3d^1$ orbitals from the LTO dopant unit cells. This conclusion is consistent with the recent experimental findings (*Appl. Phys. Lett.* **2013**, *102*, 091601). Detailed charge density and partial density of states analysis suggests that the 2DEG in the LTO-doped HS systems primarily comes from partially occupied d_{yz} and d_{xz} orbitals.

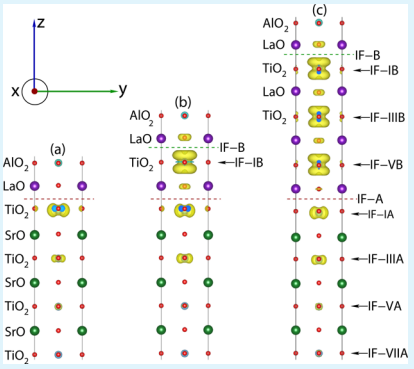

KEYWORDS: *perovskite, oxide heterostructure, 2DEG, first-principles, doping, charge carrier density*

1. INTRODUCTION

The remarkable discovery of metallic interface states and magnetism at n-type $(TiO_2)/(LaO)^{+1}$ interface between two insulating nonmagnetic perovskite oxides, polar $LaAlO_3$ (LAO) and nonpolar $SrTiO_3$ (STO), has raised intensive research interest to realize novel interfacial functionalities that are absent in the parent bulk compounds.[1−5] The TiO_2 terminated n-type $(TiO_2)^0/(LaO)^{+1}$ interfaces at LAO/STO heterostructures (HS) exhibit many spectacular phenomena such as highly mobile two-dimensional electron gas (2DEG),[1,3,4] electric-field controlled insulator-to-metal transition,[6,7] superconductivity,[8,9] and coexistence of magnetism and superconductivity.[10−12] The charge transfer from polar LAO to nonpolar STO layers at the interface, also called "polar catastrophe" mechanism, has been proposed to explain the formation of 2DEG at LAO/STO HS.[13] Meanwhile, the surface/interface defects such as oxygen vacancies[14−17] and cation-intermixing[18,19] also diversify the formation of 2DEG.

Besides the controversy surrounding the origin of 2DEG at the n-type interface between the two wide band gap insulators, LAO and STO, other related interfacial phenomena remain unclear. To demonstrate, the interfacial magnetism is not well understood at this n-type interface to date. In spite of the underlying mechanism of the magnetic ordering,[10,12,20,21] there exist a large discrepancy on the values of the magnetic moments. For instance, the magnetic moments in the LAO/STO HS-based slab system with a vacuum layer are found much smaller than that in the periodic LAO/STO HS system without a vacuum layer.[11,14,15,22] For the periodic LAO/STO HS system, about $0.5e^-$ is transferred from the LAO film to the STO substrate at the interface in order to overcome the polar discontinuity between LAO and STO. The $0.5e^-$ will partially occupy the Ti 3d orbitals, leading to a total magnetic moment of about 0.5 μ_B.[23] For the LAO/STO HS-based slab system, there exist two polar discontinuities, one at the interface and another one at the $(AlO_2)^-$ surface. The existence of bare surface $(AlO_2)^-$ layers inhibits the charge transfer from LAO to STO, and thus, with respect to the periodic LAO/STO HS system, fewer electrons are transferred to STO, leading to a relatively small magnetic moment of 0.05 μ_B on the interfacial Ti atom.[22] Pavlenko et al.[14] obtained a minute magnetic moment of about 0.005 μ_B for the interfacial Ti atoms in the LAO/STO HS-based slab system using the GGA+U scheme. Moreover, an oxygen vacancy was found of capable of enhancing the magnetic moment up to 0.34 μ_B,[14] which is in good agreement with the recent experimental value of approximately 0.3 μ_B in the oxygen-deficient LAO/STO system.[11] In contrast, Salluzzo et al. experimentally observed a relatively small magnetic moment of $1 \times 10^{-3}\mu_B$/Ti in the oxygen-annealed LAO/STO system without any oxygen

Received: December 9, 2014
Accepted: February 17, 2015
Published: February 17, 2015

DOI: 10.1021/am508662q
ACS Appl. Mater. Interfaces 2015, 7, 5305−5311

Table 1. Change in Bond Distances (Å) near the Interfacial Regions of n-type IF-A and IF-B Interfaces in LAO/(LTO)$_n$/STO (n = 0, 1, 2, and 3) HS Systems after Structural Relaxation[a]

	IF-A				IF-B		
$LaTiO_3$	Ti−O(STO)	La−O	Al−O	Ti−O(LTO)	Ti−O	La−O	Al−O
0	+0.09	−0.06	−0.04				
1	+0.07	−0.04		+0.07	+0.06	+0.01	−0.05
2	+0.06	−0.04		+0.09	+0.06	+0.03	−0.04
3	+0.04	−0.03		+0.10	+0.05	+0.05	−0.04

[a]Ti−O(STO) and Ti−O(LTO) stand for the Ti−O bond length from the STO and LTO sides near the IF-A region, respectively. Positive and negative signs indicate the increase and decrease in the bond length, respectively.

vacancies.[15] These phenomena imply that oxygen vacancies play an important role in causing interfacial magnetism.

Despite the open mechanisms of the 2DEG formation, more research efforts are being made to explore the roles of surface/interface defects,[14,15] cation-intermixing,[19] and layer doping[24−27] in tailoring the interfacial materials properties of the perovskite-based HS. One of the key physical properties of 2DEG systems is the interfacial charge carrier density, and thus tailoring two-dimensional carrier densities at the LAO/STO interfaces is essential for practical implementation in high-performance nanoelectronic devices.[13,28,29] Some experimental and theoretical efforts have been made to optimize the electron transport properties of the 2DEG in the LAO/STO HS.[23,30,31] For example, both carrier concentration and the critical thickness of LAO for forming a 2DEG at the interface can be controlled with an external electric field.[7,8,32,33] The δ-doping of strongly correlated oxides at n-type interfaces in LAO/STO HS is also an effective way to tune the physical properties of 2DEG.[24,26,34−37] Recently, Hwang et al.[25] investigated doping effects of LTO layers on the electronic properties of the LAO/STO HS and found that the 2DEG carrier density increases upon LTO doping. Moreover, the LTO-doped LAO/STO HS system was found to have the highest charge carrier density (1.3×10^{14} cm^{-2}) when a 0.25 LTO unit cell was inserted into the interface, whereas the charge carrier density decreases slightly when more LTO layers are introduced. This experimental result is interesting because it provides an avenue to tune the electronic property of the 2DEG in the perovskite-based HS by doping. Nevertheless, the atomistic origin of the enhanced charge carrier density in the LTO-layer-doped LAO/STO HS is still not fully elucidated, and it is of particular interest in the relationship between the number of LTO layers and the charge carrier density.

In this work, by using first-principles electronic structure calculations, we studied the doping effects of LTO polar layers on the electronic properties of 2DEG at the n-type $(TiO_2)^0/(LaO)^{+1}$ interfaces in $(LAO)_{4.5}/(STO)_{9.5}$ HS. Our results show that the charge carrier density of 2DEG is substantially enhanced by embedding polar LTO layers into LAO/STO HS. When the thickness of the inserted LTO layers in LAO/STO HS increases, so does that of the partial occupation of the DOS near the Fermi energy, which amplifies the charge carrier density of the 2DEG and introduces large magnetic moments.

2. COMPUTATIONAL METHODS AND STRUCTURAL MODELING

The calculations were performed in the framework of density functional theory using the Vienna Ab initio Simulation Package (VASP).[38] The spin-polarized generalized gradient approximation (GGA) parametrized by Perdew−Burke−Ernzerhof (PBE) plus on-site Coulomb interaction approach (GGA+U) was applied for the exchange-correlation functional.[39] The calculated U value of 5.8 eV for Ti 3d states from the constrained density functional theory[40] was proven high enough to describe the correct Ti 3d states.[23,41,42] A U value of 7.5 eV was used for treating strongly correlated La 4f electronic states.[43,44] The cutoff kinetic energy of 450 eV was used for the electronic wave function expansion. A $10 \times 10 \times 1$ k-space grid with 21 points in the irreducible wedge of the Brillöuin zone was found to converge appropriately. All crystal structures were optimized by minimizing the atomic forces up to 0.02 eV/Å, and self-consistency was assumed for a total energy convergence of less than 10^{-5} eV. A Gaussian smearing of 0.05 eV was used for density of states (DOS) calculations.

LAO and STO crystallize in cubic structures with a space group no. 221 ($Pm\bar{3}m$). The experimental lattice parameters and energy gaps of these compounds are 3.789 Å/3.905 Å and 5.6 eV/3.2 eV for LAO and STO, respectively.[1] The bulk pseudocubic lattice constant of LTO is 3.90 Å and its energy gap is about 0.2 eV.[45] The band gaps calculated with the GGA+U scheme were 3.12 and 2.29 eV for LAO and STO, respectively. These values are underestimated compared to the experimental values and can be correctly predicted using hybrid functional calculations.[46−49] However, the underestimation of the band gap will not alter our conclusions regarding the interfacial metallic states because the Ti 3d electronic states forming the metallic states can be well reproduced from the GGA+U calculations. Moreover, it was previously confirmed that both the GGA+U[22] and HSE06[50] methods produced similar electronic properties regarding the 2DEG in the LAO/STO HS system. This indicates that the GGA+U approach is reliable in predicting Ti 3d orbital-related electronic states. A pseudocubic unit cell of LTO is used in all the present calculations, with the lattice mismatch between LAO and LTO at 2.9%, whereas that between LTO and STO is only 0.13%. Hence, LTO has a nearly perfect lattice match with STO and LAO, therefore is a good choice of δ-doped polar layers for LAO/STO HS to enhance electron conductivity. A supercell approach is used to model the periodic $(LAO)_{4.5}/(LTO)_n/(STO)_{9.5}$ (n = 0, 1, 2, and 3) HS systems, which contain two symmetrical $(LaO)^{+1}/(TiO_2)^0$ n-type interfaces. The experimental lattice constants of the STO substrate is fixed in the ab-plane to model the interfacial supercells in each case.

3. RESULTS AND DISCUSSION

3.1. Structural Relaxation. It is experimentally and theoretically[51,52] observed that at and near the interfacial region, the electronic states critically rely on structural details and different structural relaxation patterns are found for change in bond distances. Therefore, it is important to fully relax the structures by minimizing the atomic forces. After introducing LTO layers in the LAO/STO HS, two n-type $(LaO)^{+1}/(TiO_2)^0$ interfaces form in the supercell. One is between the STO substrate and the LTO layer, labeled as IF-A, and the other is between the LTO and LAO layers, labeled as IF-B, as discussed in charge density plots section. The calculated bond lengths near the interfacial regions of IF-A and IF-B are summarized in Table 1. Positive and negative signs indicate the respective increase and decrease in the bond lengths as compared with

DOI: 10.1021/am508662q
ACS Appl. Mater. Interfaces 2015, 7, 5305−5311

that in the unrelaxed system. For the undoped HS system, a substantial distortion is observed in TiO_6 octahedra near the interfacial region. Our structural relaxation indicates that near the IF-A region, Ti−O and La−O/Al−O bond lengths increased and decreased along the *c*-direction, respectively. After doping with LTO layers, Ti−O and La−O bond lengths decrease and show less distortion along the *c*-direction as compared to that in the undoped system. On the other hand, Al−O bond lengths remain almost identical to those found in the undoped system, and thus are not listed here. In contrast, the Ti−O bond length (in the LTO) near the IF-A region substantially increases as the number of the LTO layers increase. At the IF-B region, as the number of LTO layers increases, the Ti−O bond length (in the LTO side) show nearly the same distortion, whereas La−O bond length increases. Furthermore, the angles between O−Ti−O in the *ab*-plane at the IF-IA/IF-IB TiO_2 layers are 172.4, 172.1/177.4, 171.8/176.2, and 171.3/175.8° for LAO/$(LTO)_n$/STO (n = 0, 1, 2, and 3) HS systems, respectively. One can clearly see that as the number of LTO doped layers is increased, the TiO_6 octahedra becomes proportionally distorted in both the STO and LTO sides, as compared to the undoped system despite the degree of distortion being less. Additionally, the degree of TiO_6 distortion in STO is higher than that in the LTO side.

3.2. Undoped LAO/STO Heterostructure. To explicitly show the doping effects of LTO layer on the electronic and magnetic properties of LAO/STO HS system, we first analyzed the electronic structure of the undoped LAO/STO HS system to provide a frame of reference. We focused on the Ti 3d orbitals, as it is established that these orbitals are the primary constituents of the interfacial metallic states and form the 2DEG in STO-based HS systems.[23] The calculated total and partial DOS projected on Ti 3d orbitals from three consecutive interfacial TiO_2 layers in the STO substrate is shown in panels a and b in Figure 1, respectively. The total DOS in Figure 1a clearly exhibits typical n-type conductivity with a wide band gap

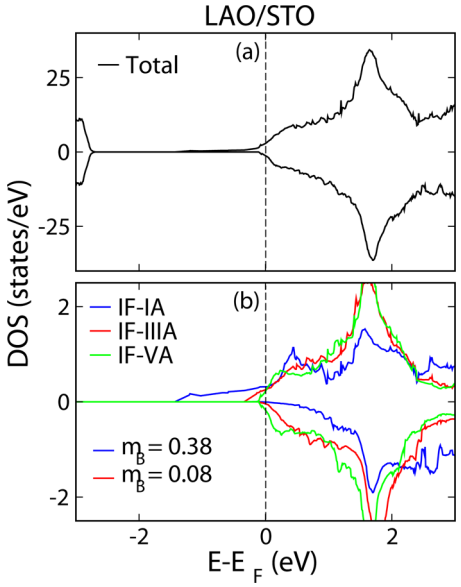

Figure 1. Calculated spin-polarized (a) total and (b) partial Ti 3d DOS at the $(LaO)^{+1}/(TiO_2)^0$ n-type interface in an undoped LAO/STO HS system near the interfacial region of STO. The Fermi level is indicated by the vertical dashed line at 0 eV. IF-IA, IF-IIIA, and IF-VA represent the first, third and fifth TiO_2 layers in STO, respectively.

of ∼2.7 eV. For the partial Ti 3d DOS (Figure 1b), the first, third, and fifth TiO_2 layers of STO are designated IF-I, IF-III, and IF-V, respectively. One can see that most of the metallic states near the Fermi level come from the first TiO_2 layer (IF-I) of the STO substrate along with a small contribution from the third (IF-III) and fifth (IF-V) TiO_2 layers. Additional partial DOS analysis indicates that other layers away from the interface nearly show an insulating behavior, which confirms the formation of a 2DEG. This means that the charge transferred from the polar $(LaO)^{+1}$ layer to the nonpolar TiO_2 layers predominantly occupies the Ti sites and resides only in the top few layers of the STO substrate (∼3 unit cells of the STO), showing that the width of the metallic region in this HS system is ∼9.6 Å. Furthermore, the interfacial (IF-I) TiO_2 layer exhibits a nearly half-metallic nature with a magnetic moment of 0.38 μ_B on the Ti atom. The calculated magnetic moment of the Ti atom in the IF-III TiO_2 layer is 0.08 μ_B and all other layers further away from the interface exhibit no spin-polarization.[23] Our calculated magnetic moments are in excellent agreement with the previously reported values of interfacial Ti atoms in LAO/STO HS systems within the GGA+U scheme.[53] Moreover, Pickett et al.[43] found a strong charge localization at the interfacial TiO_2 layer in the LAO/STO HS when performing calculations with the GGA+U method as compared to GGA, which support our conclusion for an undoped n-type interface.

3.3. LTO-Doped LAO/STO Heterostructures. Next, we studied the doping effects of LTO layers on the electronic properties of the 2DEG in the LAO/STO HS. The calculated total and partial DOS projected on Ti 3*d* orbitals near the interfacial region, as discussed in Figure 1b for LAO/$(LTO)_n$/STO (n = 1 and 3), are shown in Figure 2. The total DOS for n = 1 (Figure 2a) and 3 (Figure 2b) HS systems indicate that the orbital occupation near the Fermi energy increases as compared to that in the undoped system (Figure 1a). The LTO layers introduce additional Ti 3d electrons into the system, which partially occupy Ti 3d orbitals, and thus significantly modify the electronic states near the Fermi level, resulting in an enhancement of the charge carrier density of the system. From the partial DOS, one can see that the Ti 3d orbitals near the n-type IF-A region (Figure 2c) of the LAO/$(LTO)_1$/STO system shows almost same occupation as found in the case of the undoped system (Figure 1b). The Ti 3d orbitals from the IF-IA TiO_2 layer of the STO substrate are primarily responsible for the conductivity along with a small contribution from the IF-IIIA and IF-VA layers (Figure 2c).

Similarly, the calculated magnetic moments of the Ti atoms in the IF-IA and IF-IIIA TiO_2 layers are almost identical to those in the undoped LAO/STO system. On the other hand, Ti 3d orbitals from the IF-IB TiO_2 layer (Figure 2b) exhibit much higher occupation than that from the IF-IA layer, resulting in higher total charge carrier density and larger magnetic moment of the system. For the LAO/$(LTO)_3$/STO HS system, the Ti 3d states from the IF-IA layer shift toward higher energy, whereas that from the IF-IIIA layer shift toward lower energy. This makes the partial occupation of 3d orbitals at the IF-IA and IF-IIIA layers slightly decrease and increase, respectively. As a result, the magnetic moment of the Ti ion from the IF-IA layer decreases to 0.35 μ_B, whereas that from the IF-IIIA layer increases to 0.10 μ_B. In contrast, the Ti 3d orbitals at IF-IB, IF-IIIB, and IF-VB TiO_2 layers substantially shift (∼0.6 eV) toward lower energy as compared to the LAO/$(LTO)_1$/STO system, and the band edges of Ti 3d states from these three layers are nearly at the same position despite of the slight

DOI: 10.1021/am508662q
ACS Appl. Mater. Interfaces 2015, 7, 5305−5311

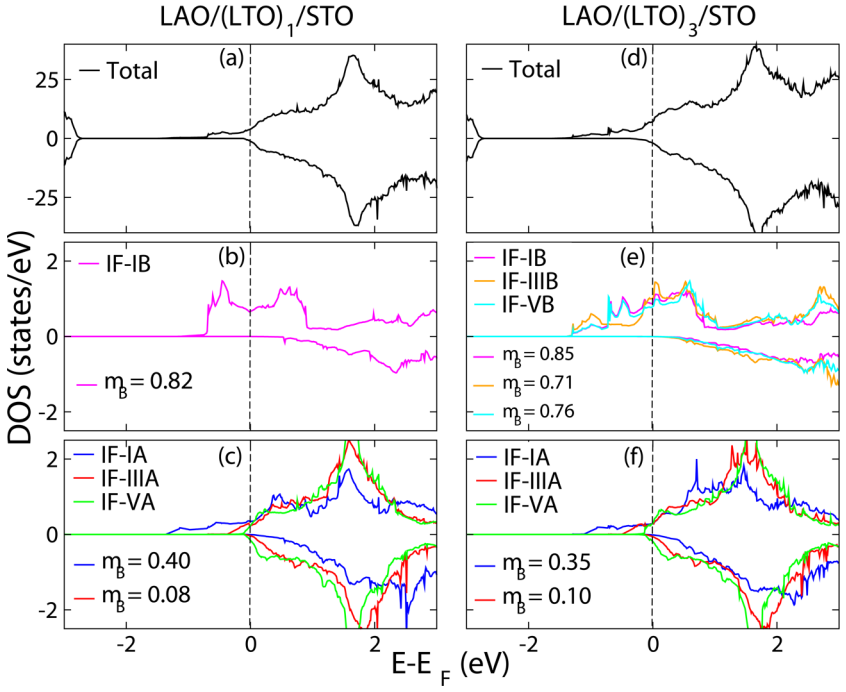

Figure 2. Calculated spin-polarized (a, d) total and (b, c, e, f) partial Ti 3d DOS at $(LaO)^{+1}/(TiO_2)^0$ n-type interfaces in LAO/$(LTO)_n$/STO (n = 1 and 3) HS systems near the interfacial region of STO and LTO. IF-IA(IB), IF-IIIA(IIIB), and IF-VA(VB) represent the first, third, and fifth TiO_2 layers in STO(LTO), respectively.

difference of the occupation number. Our results show that the magnetic moment on the Ti atom at the IF-IB TiO_2 layer is slightly higher (0.85 μ_B) than that of the other layers (Figure 2e).

3.4. Charge Density. To fully understand the behavior of the metallic interface states with respect to the LTO layers, we plotted the charge density projected on the bands that form the 2DEG for LAO/$(LTO)_n$/STO (n = 0, 1, and 3) HS systems in Figure 3. Our results clearly indicate that for undoped (n = 0) LAO/STO HS systems, electrons transferred from the polar $(LaO)^{+1}$ layer extend to the deeper $(TiO_2)^0$ layers of the STO substrate (~3 unit cells), see Figure 3a.

This is consistent with the calculated DOS in Figure 1b. For the LTO doped LAO/STO system, a slight decrease is found in the density of the IF-IA TiO_2 layer as compared to that of undoped system, whereas the IF-IB, IF-IIIB, and IF-VB TiO_2 layers exhibit a larger and nearly constant density (see Figure 3b, c). In short, one can conclude that inserting the LTO layers between the LAO and STO layers can significantly modify the electronic property of the LAO/STO HS system. In addition, from Figure 3, one can see that the occupied Ti 3d orbitals in STO and LTO differ in shape. This means that the 3d bands, which form the 2DEG in LAO/LTO/STO HS systems, have different orbital occupations. To further verify this conclusion, we plotted the orbital-resolved DOS of Ti 3d states at IF-IA and IF-IB for the LAO/$(LTO)_1$/STO HS system in Figure 4.

It is well-known that in a regular octahedral crystal field, Ti 3d states are split into triply t_{2g} (d_{xy}, d_{xz}, and d_{yz}) and doubly e_g ($d_{3z^2-r^2}$ and $d_{x^2-y^2}$) degenerate states. After structural relaxation, the distortion of the TiO_6 unit in the HS results in a degraded symmetry, and the triply degenerate t_{2g} states are split into nondegenerate d_{xy}, d_{yz}, and d_{zx} orbitals. From Figure 4a, one can clearly see that only d_{xy} orbitals cross the Fermi level at the IF-IA interface in the STO substrate and are thus singularly responsible for the 2DEG, whereas the d_{yz}/d_{xz} orbital remain

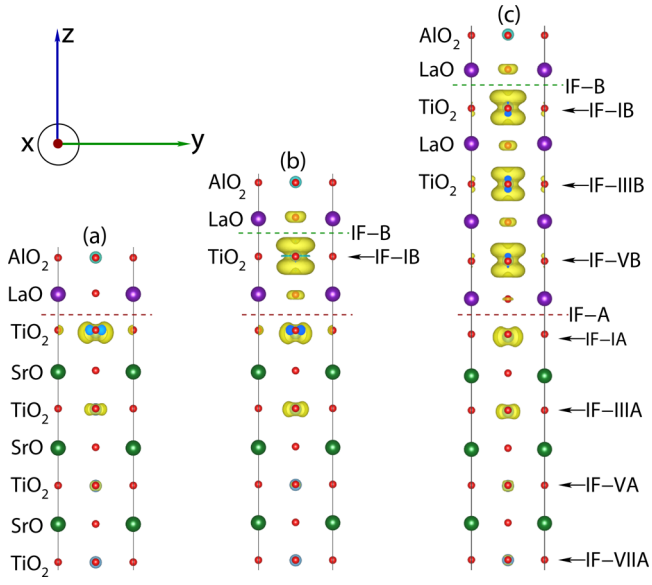

Figure 3. Charge density plots projected on the bands forming the 2DEG at the LAO/$(LTO)_n$/STO HS for (a) n = 0 (undoped), (b) n = 1, and (c) n = 3. IF-IA and IF-IB represent the n-type interfaces at LTO/STO and LTO/LAO in LAO/$(LTO)_n$/STO HS systems, respectively. The same isovalue of 0.0038 is used to produce the charge density plots. The x, y, and z axes are along the crystallographic a, b, and c directions, respectively. The x-axis (a-direction) is pointing toward the observer.

unoccupied. A similar observation has confirmed[54,55] that 2DEG reside in the ab-plane in LAO(LTO)/STO HS systems. In contrast, at IF-IB interface in the LTO layers, the metallicity results from the admixture of d_{yz} and d_{xz} orbitals. The d_{yz} and d_{xz} orbitals are the primary contributors to the system conductivity. In contrast, d_{xy} orbitals remain unoccupied and

DOI: 10.1021/am508662q
ACS Appl. Mater. Interfaces 2015, 7, 5305−5311

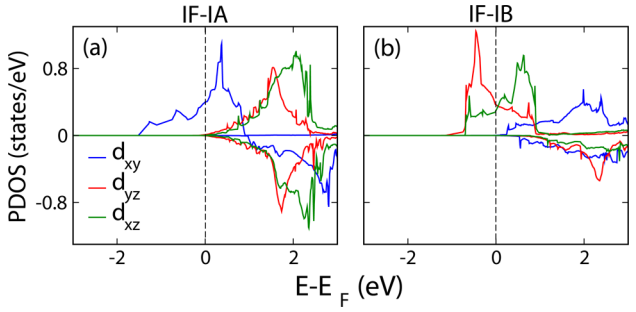

Figure 4. Orbitally resolved partial DOS of Ti 3d orbitals at $(LaO)^{+1}/(TiO_2)^0$ n-type interfaces from (a) IF-IA (in STO side) and (b) IF-IB (in LTO side) TiO_2 layers in LAO/$(LTO)_1$/STO HS system, respectively.

stay at higher energies in the conduction band (far away from the Fermi level), see Figure 4b.

3.5. Interfacial Charge Carrier Density. To obtain a qualitative comparison of the charge carrier density for LAO/$(LTO)_n$/STO (n = 0, 1, 2, and 3) HS systems, we calculated their occupation number by integrating the total and partially occupied Ti 3d DOS on the IF-IA and IF-IB TiO_2 layers and then proceeded to determine the charge carrier density in each system. The estimated partial occupations of the total DOS are 0.95, 1.96, 2.98, and 3.82 for the LAO/STO, LAO/$(LTO)_1$/STO, LAO/$(LTO)_2$/STO, and LAO/$(LTO)_3$/STO HS systems, respectively. The computed total Ti 3d charge carrier densities from estimated values of their occupation numbers with respect to LTO unit cells is plotted in Figure 5. Our

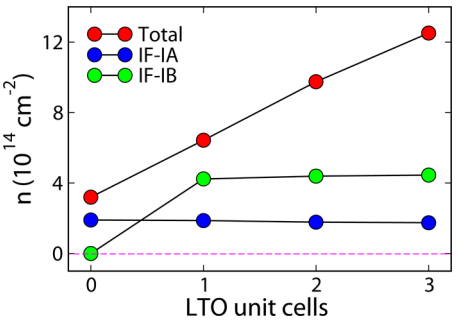

Figure 5. Calculated total and Ti 3d charge carrier densities from IF-IA (in STO side) and IF-IB (in LTO side) TiO_2 layers at n-type interfaces in LAO/$(LTO)_n$/STO (n = 0, 1, 2, and 3) HS systems with respect to LTO unit cells.

theoretical calculations reveal that charge carrier densities substantially enhanced when LTO layers are inserted into LAO/STO HS, which is in agreement with recent experimental findings.[25] Hwang et al., found an increase in carrier density ($\sim 1.3 \times 10^{14}$ cm^{-2}) when a 0.25 unit cell of LTO was inserted into LAO/STO HS. However, they also observed that the total charge carrier density slightly decreases when more than 0.25 LTO unit cells are introduced. This is inconsistent with our calculations. Our results reveal that inserting the LTO layer into the LAO/STO HS provides one extra electron from Ti $3d^1$ orbital per LTO unit cell, which results in an enhancement of the charge carrier density. As a result, as confirmed from our theoretical calculations, the total charge carrier density increases as the increase of the LTO layers. Moreover, our calculations indicate that the carrier density at IF-IA and IF-IB is nearly constant, which is consistent with the DOS in Figures 1 and 2c. This is because the orbital occupation of the Ti 3d states from the IF-IA (in STO side) and IF-IB (in LTO side) TiO_2 layers is almost identical. This conclusion is also reinforced by the charge density plots, illustrated in Figure 3. Hence, more detailed experimental studies are desired to explore the dependence of the total charge carrier density on the number of the LTO layers. Moreover, it is also noted that the experimentally observed charge carrier density[1,6,56,57] at undoped n-type interface in LAO/STO HS systems is lower than the theoretically calculated[23,58] values, probably caused by the discrepancy of the structural model.

4. CONCLUSION

In summary, spin-polarized density functional theory calculations were performed to examine the origin of enhanced charge-carrier density in LAO/STO HS with inserted LTO layers. Our results predict that by doping LTO layers in LAO/STO HS, the number of the partially occupied Ti 3d orbitals near the Fermi energy increases, which leads to a higher charge carrier density than that of the undoped system. This is because the LTO unit cell provides an extra electron from its Ti 3d orbitals to the system. Our calculations also reveal that the electrons forming the 2DEG in the LTO unit cells reside in the yz and xz-plane instead of xy-plane as found in the STO substrate. This implies that the 2DEG comes from the partially occupied d_{yz} and d_{xz} orbitals instead of the d_{xy} orbitals.

AUTHOR INFORMATION

Corresponding Author

*E-mail: kesong@ucsd.edu. Phone: +1-858-534-2514.

Notes

The authors declare no competing financial interest.

ACKNOWLEDGMENTS

This work is partially supported by ONR (N000141510030). K.Y. acknowledges support by start-up funds from the University of California, San Diego.

REFERENCES

(1) Ohtomo, A.; Hwang, H. Y. A High-Mobility Electron Gas at the $LaAlO_3/SrTiO_3$ Heterointerface. *Nature* **2004**, *427*, 423−426.

(2) Brinkman, A.; Huijben, M.; van Zalk, M.; Huijben, J.; Zeitler, U.; Maan, J. C.; van der Wiel, W. G.; Rijnders, G.; Blank, D. H. A.; Hilgenkamp, H. Magnetic Effects at the Interface between Non-Magnetic Oxides. *Nat. Mater.* **2007**, *6*, 493−496.

(3) Lesne, E.; Reyren, N.; Doennig, D.; Mattana, R.; Jaffrés, H.; V.Cros, F. P.; Choueikani, F.; Ohresser, P.; Pentcheva, R.; Barthélémy, A.; Bibes, M. Suppression of the Critical Thickness Threshold for Conductivity at the $LaAlO_3/SrTiO_3$ Interface. *Nat. Commun.* **2012**, *5*, 4291.

(4) Mannhart, J.; Schlom, D. G. Oxide Interfaces-An Opportunity for Electronics. *Science* **2010**, *327*, 1607−1611.

(5) Kalisky, B.; Bert, J. A.; Klopfer, B. B.; Bell, C.; Sato, H. K.; Hosoda, M.; Hikita, Y.; Hwang, H. Y.; Moler, K. A. Critical Thickness for Ferromagnetism in $LaAlO_3/SrTiO_3$ Heterostructures. *Nat. Commun.* **2012**, *3*, 922.

(6) Thiel, S.; Hammerl, G.; Schmehl, A.; Schneider, C. W.; Mannhart, J. Tunable Quasi-Two-Dimensional Electron Gases in Oxide Heterostructures. *Science* **2006**, *313*, 1942−1945.

(7) Caviglia, A. D.; Gariglio, S.; Reyren, N.; Jaccard, D.; Schneider, T.; Gabay, M.; Thiel, S.; Hammerl, G.; Mannhart, J.; Triscone, J. M. Electric Field Control of the $LaAlO_3/SrTiO_3$ Interface Ground State. *Nature* **2008**, *456*, 624−627.

DOI: 10.1021/am508662q
ACS Appl. Mater. Interfaces 2015, 7, 5305−5311

(8) Reyren, N.; Thiel, S.; Caviglia, A. D.; Kourkoutis, L. F.; Hammer, G.; Richter, C.; Schneider, C. W.; Kopp, T.; Rüetschi, A. S.; Jaccard, D.; Gabay, M.; Muller, D. A.; Triscone, J. M.; Mannhart, J. Superconducting Interfaces Between Insulating Oxides. *Science* **2007**, *317*, 1196−1199.
(9) Ben Shalom, M.; Sachs, M.; Rakhmilevitch, D.; Palevski, A.; Dagan, Y. Tuning Spin-Orbit Coupling and Superconductivity at the $SrTiO_3/LaAlO_3$ Interface: A Magnetotransport Study. *Phys. Rev. Lett.* **2010**, *104*, 126802.
(10) Bert, J. A.; Kalisky, B.; Bell, C.; Kim, M.; Hikita, Y.; Hwang, H. Y.; Moler, K. A. Direct Imaging of the Coexistence of Ferromagnetism and Superconductivity at the $LaAlO_3/SrTiO_3$ Interface. *Nat. Phys.* **2011**, *7*, 767−771.
(11) Li, L.; Richter, C.; Mannhart, J.; Ashoori, R. C. Coexistence of Magnetic Order and Two-Dimensional Superconductivity at $LaAlO_3/SrTiO_3$ Interfaces. *Nat. Phys.* **2011**, *7*, 762−766.
(12) Lee, J. S.; Xie, Y. W.; Sato, H. K.; Bell, C.; Hikita, Y.; Hwang, H. Y.; Kao, C. C. Titanium d_xy Ferromagnetism at the $LaAlO_3/SrTiO_3$ Interface. *Nat. Mater.* **2013**, *12*, 703−706.
(13) Cen, C.; Thiel, S.; Hammerl, G.; Schneider, C. W.; Andersen, K. E.; Hellberg, C. S.; Mannhart, J.; Levy, J. Nanoscale Control of an Interfacial Metal-Insulator Transition at Room Temperature. *Nat. Mater.* **2008**, *7*, 298−302.
(14) Pavlenko, N.; Kopp, T.; Tsymbal, E. Y.; Sawatzky, G. A.; Mannhart, J. Magnetic and Superconducting Phases at the $LaAlO_3/SrTiO_3$ Interface: The Role of Interfacial Ti 3*d* Electrons. *Phys. Rev. B* **2012**, *85*, 020407.
(15) Salluzzo, M.; Gariglio, S.; Stornaiuolo, D.; Sessi, V.; Rusponi, S.; Piamonteze, C.; De Luca, G. M.; Minola, M.; Marré, D.; Gadaleta, A.; Brune, H.; Nolting, F.; Brookes, N. B.; Ghiringhelli, G. Origin of Interface Magnetism in $BiMnO_3/SrTiO_3$ and $LaAlO_3/SrTiO_3$ Heterostructures. *Phys. Rev. Lett.* **2013**, *111*, 087204.
(16) Yu, L.; Zunger, A. A Polarity-Induced Defect Mechanism for Conductivity and Magnetism at Polar-Nonpolar Oxide Interfaces. *Nat. Commun.* **2014**, *5*, 5118.
(17) Liu, Z.; Li, C.; Lü, W.; Huang, X.; Huang, Z.; Zeng, S.; Qiu, X.; Huang, L.; Annadi, A.; Chen, J.; Coey, J.; Venkatesan, T. Ariando, Origin of the Two-Dimensional Electron Gas at $LaAlO_3/SrTiO_3$ Interfaces: The Role of Oxygen Vacancies and Electronic Reconstruction. *Phys. Rev. X* **2013**, *3*, 021010.
(18) Nakagawa, N.; Hwang, H. Y.; Muller, D. A. Why Some Interfaces Cannot be Sharp. *Nat. Mater.* **2006**, *5*, 204−209.
(19) Qiao, L., Droubay, T. C., Shutthanandan, V., Zhu, Z., Sushko, P. V., Chambers, S. A. Thermodynamic Instability at the Stoichiometric $LaAlO_3/SrTiO_3$ (001) Interface *J. Phys. Conden. Matt.* **2010**, *22*, 312201.
(20) Dikin, D. A.; Mehta, M.; W, C.; Folkman, C. M.; Eom, C. B.; Chandrasekhar, V. Coexistence of Superconductivity and Ferromagnetism in Two Dimensions. *Phys. Rev. Lett.* **2011**, *107*, 056802.
(21) Salman, Z.; et al. Nature of Weak Magnetism in $SrTiO_3/LaAlO_3$ Multilayers. *Phys. Rev. Lett.* **2012**, *109*, 257207.
(22) Nazir, S.; Yang, K. First-Principles Characterization of the Critical Thickness for Forming Metallic States in Strained $LaAlO_3/SrTiO_3$(001) Heterostructure. *ACS Appl. Mater. Interfaces* **2014**, *6*, 22351−22358.
(23) Nazir, S.; Behtash, M.; Yang, K. Enhancing Interfacial Conductivity and Spatial Charge Confinement of $LaAlO_3/SrTiO_3$ Heterostructures via Strain Engineering. *Appl. Phys. Lett.* **2014**, *105*, 141602.
(24) Frank, S.; Michael, A. C.; Mary, E. V.; Mehmet, E.; Thomas, F.; Josee, E. K.; Judith, L. M. D.; Mark, G. B. Carrier Density Modulation by Structural Distortions at Modified $LaAlO_3/SrTiO_3$ Interfaces. *J. Phys. Conden. Matt.* **2013**, *25*, 175005.
(25) Hosoda, M.; Bell, C.; Hikita, Y.; Hwang, H. Y. Compositional and Gate Tuning of the Interfacial Conductivity in $LaAlO_3/LaTiO_3/SrTiO_3$ Heterostructures. *Appl. Phys. Lett.* **2013**, *102*, 091601.
(26) De Luca, G. M.; Di Capua, R.; Di Gennaro, E.; Granozio, F. M.; Stornaiuolo, D.; Salluzzo, M.; Gadaleta, A.; Pallecchi, I.; Marrè, D.; Piamonteze, C.; Radovic, M.; Ristic, Z.; Rusponi, S. Transport Properties of a Quasi-Two-Dimensional Electron System Formed in $LaAlO_3/EuTiO_3/SrTiO_3$ Heterostructures. *Phys. Rev. B* **2014**, *89*, 224413.
(27) Disa, A. S.; Kumah, D. P.; Malashevich, A.; Chen, H.; Arena, D. A.; Specht, E. D.; Ismail-Beigi, S.; Walker, F. J.; Ahn, C. H. Orbital Engineering in Symmetry-Breaking Polar Heterostructures. *Phys. Rev. Lett.* **2015**, *114*, 026801.
(28) Cen, C.; Thiel, S.; Mannhart, J.; Levy, J. Oxide Nanoelectronics on Demand. *Science* **2009**, *323*, 1026−1030.
(29) Stornaiuolo, D.; Gariglio, S.; Fête, A.; Gabay, M.; Li, D.; Massarotti, D.; Triscone, J.-M. Weak Localization and Spin-Orbit Interaction in Side-Gate Field Effect Devices at the $LaAlO_3/SrTiO_3$ Interface. *Phys. Rev. B* **2014**, *90*, 235426.
(30) Bark, C. W.; Felker, D. A.; Wang, Y.; Zhang, Y.; Jang, H. W.; Folkman, C. M.; Park, J. W.; Baek, S. H.; Zhou, H.; Fong, D. D.; Pan, X. Q.; Tsymbal, E. Y.; Rzchowski, M. S.; Eom, C. B. Tailoring a Two-Dimensional Electron Gas at the $LaAlO_3/SrTiO_3$ (001) Interface by Epitaxial Strain. *Proc. Natl. Acad. Sci. U.S.A* **2011**, *108*, 4720−4724.
(31) Kalisky, B.; et al. Locally Enhanced Conductivity Due to the Tetragonal Domain Structure in $LaAlO_3/SrTiO_3$ Heterointerfaces. *Nat. Mater.* **2013**, *12*, 1091−1095.
(32) Yajima, T.; Hikita, Y.; Hwang, H. Y. A Heteroepitaxial Perovskite Metal-Base Transistor. *Nat. Mater.* **2011**, *10*, 198−201.
(33) Rastogi, A.; Kushwaha, A. K.; Shiyani, T.; Gangawar, A.; Budhani, R. C. Electrically Tunable Optical Switching of a Mott Insulator-Band Insulator Interface. *Adv. Mater.* **2010**, *22*, 4448−4451.
(34) Fix, T.; MacManus-Driscoll, J. L.; Blamire, M. G. Delta-Doped $LaAlO_3/SrTiO_3$ Interfaces. *Appl. Phys. Lett.* **2009**, *94*, 172101.
(35) Ong, P. V.; Lee, J.; Pickett, W. E. Tunable Two-Dimensional or Three-Dimensional Electron Gases by Submonolayer La Doping of $SrTiO_3$. *Phys. Rev. B* **2011**, *83*, 193106.
(36) Choi, W. S.; Lee, S.; Cooper, V. R.; Lee, H. N. Fractionally δ-Doped Oxide Superlattices for Higher Carrier Mobilities. *Nano Lett.* **2012**, *12*, 4590−4594.
(37) Rastogi, A.; Pulikkotil, J. J.; Budhani, R. C. Enhanced Persistent Photoconductivity in δ-Doped $LaAlO_3/SrTiO_3$ Heterostructures. *Phys. Rev. B* **2014**, *89*, 125127.
(38) Kresse, G.; Furthmüller, J. Efficient Iterative Schemes for *ab initio* Total-Energy Calculations using a Plane-Wave Basis Set. *Phys. Rev. B* **1996**, *54*, 11169−11186.
(39) Perdew, J. P.; Burke, K.; Ernzerhof, M. Generalized Gradient Approximation Made Simple. *Phys. Rev. Lett.* **1996**, *77*, 3865−3868.
(40) Anisimov, V. I.; Zaanen, J.; Andersen, O. K. Band Theory and Mott insulators: Hubbard *U* instead of Stoner. *I. Phys. Rev. B* **1991**, *44*, 943−954.
(41) Yang, K.; Dai, Y.; Huang, B.; Feng, Y. P. Density Functional Characterization of the Antiferromagnetism in Oxygen-Deficient Anatase and Rutile TiO_2. *Phys. Rev. B* **2010**, *81*, 033202.
(42) Kesong, Y.; Ying, D.; Baibiao, H.; Yuan, P. F. First-Principles GGA+*U* Study of the Different Conducting Properties in Pentavalent-Ion-Doped Anatase and Rutile TiO_2. *J. Phys. D: Appl. Phys.* **2014**, *47*, 275101.
(43) Pentcheva, R.; Pickett, W. E. Ionic Relaxation Contribution to the Electronic Reconstruction at the *n*-Type $LaAlO_3/SrTiO_3$ Interface. *Phys. Rev. B* **2008**, *78*, 205106.
(44) Arras, R.; Ruiz, V. G.; Pickett, W. E.; Pentcheva, R. Tuning the Two-Dimensional Electron Gas at the $LaAlO_3/SrTiO_3$(001) Interface by Metallic Contacts. *Phys. Rev. B* **2012**, *85*, 125404.
(45) Okimoto, Y.; Katsufuji, T.; Okada, Y.; Arima, T.; Tokura, Y. Optical Spectra in $(La,Y)TiO_3$: Variation of Mott-Hubbard Gap Features with Change of Electron Correlation and Band Filling. *Phys. Rev. B* **1995**, *51*, 9581−9588.
(46) Janesko, B. G.; Henderson, T. M.; Scuseria, G. E. Screened Hybrid Density Functionals for Solid-State Chemistry and Physics. *J. Phys. Condens. Matter* **2009**, *11*, 443−454.
(47) El-Mellouhi, F.; Brothers, E. N.; Lucero, M. J.; Scuseria, G. E. Modeling of the Cubic and Antiferrodistortive Phases of $SrTiO_3$ with Screened Hybrid Density Functional Theory. *Phys. Rev. B* **2011**, *84*, 115122.

DOI: 10.1021/am508662q
ACS Appl. Mater. Interfaces 2015, 7, 5305−5311

(48) El-Mellouhi, F.; Brothers, E. N.; Lucero, M. J.; Bulik, I. W.; Scuseria, G. E. Structural Phase Transitions of the Metal Oxide Perovskites $SrTiO_3$, $LaAlO_3$, and $LaTiO_3$ Studied with a Screened Hybrid Functional. *Phys. Rev. B* **2013**, *87*, 035107.
(49) Franchini, C. Hybrid Functionals Applied to Perovskites. *J. Phys.: Conden. Matt.* **2014**, *26*, 253202.
(50) Cossu, F.; Schwingenschlögl, U.; Eyert, V. Metal-Insulator Transition at the $LaAlO_3/SrTiO_3$ Interface Revisited: A Hybrid Functional Study. *Phys. Rev. B* **2013**, *88*, 045119.
(51) Okamoto, S.; Millis, A. J.; Spaldin, N. A. Lattice Relaxation in Oxide Heterostructures: $LaTiO_3/SrTiO_3$ Superlattices. *Phys. Rev. Lett.* **2006**, *97*, 056802.
(52) Hamann, D. R.; Muller, D. A.; Hwang, H. Y. Lattice-Polarization Effects on Electron-Gas Charge Densities in Ionic Superlattices. *Phys. Rev. B* **2006**, *73*, 195403.
(53) Janicka, K.; Velev, J. P.; Tsymbal, E. Y. Magnetism of $LaAlO_3/SrTiO_3$ Superlattices. *J. Appl. Phys.* **2008**, *103*, 07B508.
(54) Salluzzo, M.; Cezar, J. C.; Brookes, N. B.; Bisogni, V.; De Luca, G. M.; Richter, C.; Thiel, S.; Mannhart, J.; Huijben, M.; Brinkman, A.; Rijnders, G.; Ghiringhelli, G. Orbital Reconstruction and the Two-Dimensional Electron Gas at the $LaAlO_3/SrTiO_3$ Interface. *Phys. Rev. Lett.* **2009**, *102*, 166804.
(55) You, J. H.; Lee, J. H. Critical Thickness for the Two-Dimensional Electron Gas in $LaTiO_3/SrTiO_3$ Superlattices. *Phys. Rev. B* **2013**, *88*, 155111.
(56) Huijben, M.; Rijnders, G.; Blank, D. H. A.; Bals, S.; Aert, S. V.; Verbeeck, J.; Tendeloo, G. V.; Brinkman, A.; Hilgenkamp, H. Electronically Coupled Complementary Interfaces Between Perovskite Band Insulators. *Nat. Mater.* **2006**, *5*, 556−560.
(57) Kalabukhov, A.; Gunnarsson, R.; Börjesson, J.; Olsson, E.; Claeson, T.; Winkler, D. Effect of Oxygen Vacancies in the $SrTiO_3$ Substrate on the Electrical Properties of the $LaAlO_3/SrTiO_3$ Interface. *Phys. Rev. B* **2007**, *75*, 121404.
(58) Son, W.-J.; Cho, E.; Lee, B.; Lee, J.; Han, S. Density and Spatial Distribution of Charge Carriers in the Intrinsic n-type $LaAlO_3$-$SrTiO_3$ Interface. *Phys. Rev. B* **2009**, *79*, 245411.

DOI: 10.1021/am508662q
ACS Appl. Mater. Interfaces 2015, 7, 5305−5311